

## MIT Open Access Articles

*Mercury-induced aggregation of human lens #-  
crystallins reveals a potential role in cataract disease*

The MIT Faculty has made this article openly available. **Please share**  
how this access benefits you. Your story matters.

**As Published:** <https://doi.org/10.1007/s00775-018-1607-z>

**Publisher:** Springer Berlin Heidelberg

**Persistent URL:** <https://hdl.handle.net/1721.1/131298>

**Version:** Author's final manuscript: final author's manuscript post peer review, without publisher's formatting or copy editing

**Terms of Use:** Article is made available in accordance with the publisher's policy and may be subject to US copyright law. Please refer to the publisher's site for terms of use.



# **Mercury-induced aggregation of human lens $\gamma$ -crystallins reveals a potential role in cataract disease**

J. A. Domínguez-Calva,<sup>1</sup> M. L. Pérez-Vázquez,<sup>1</sup> E. Serebryany,<sup>2</sup> J. A. King,<sup>2</sup> L. Quintanar,<sup>1,\*</sup>

<sup>1</sup>Departamento de Química, Centro de Investigación y de Estudios Avanzados (Cinvestav), Mexico City, México

<sup>2</sup>Department of Biology, Massachusetts Institute of Technology, Cambridge, MA, USA

[lilianaq@cinvestav.mx](mailto:lilianaq@cinvestav.mx)

Keywords: lens crystallins, human gamma crystallin, mercury, heavy metal ions, cataract disease

## **Abstract**

Cataract disease results from non-amyloid aggregation of eye lens proteins and it is the leading cause of blindness in the world. A variety of studies have implicated both essential and xenobiotic metals as potential etiological agents in cataract disease. Essential metal ions, such as copper and zinc, are known to induce the aggregation *in vitro* of human  $\gamma$ D-crystallin, one of the more abundant  $\gamma$ -crystallins in the core of the lens. In this study, we expand the investigation of metal-crystallin interactions to heavy metal ions, such as divalent lead, cadmium and mercury. The impact of these metal ions in the non-amyloid aggregation, protein folding and thermal stability of three homologous human lens  $\gamma$ -crystallins has been evaluated using turbidity assays, electron microscopy, electronic absorption and circular dichroism spectroscopies. Our results show that Hg(II) ions can induce the non-amyloid aggregation of human  $\gamma$ C- and  $\gamma$ S-crystallins, but not  $\gamma$ D-crystallin. The mechanism of Hg-induced aggregation involves direct metal-protein interactions, loss of thermal stability, partial unfolding of the N-terminal domain of these proteins, and formation of disulfide-bridged dimers. Putative Hg(II) binding sites in  $\gamma$ -crystallins involved in metal-induced aggregation are discussed. This study reveals that mercury ions can induce the aggregation of human lens proteins, uncovering a potential role of this heavy metal ion in the bioinorganic chemistry of cataract disease.

## Introduction

Cataract disease is the number one cause of blindness in the world, affecting over 60 million people worldwide [1]. Cataracts are formed upon aggregation of lens proteins into light-scattering high molecular weight complexes that cause lens opacity. Human lens transparency depends on the solubility and stability of crystallins, the most abundant proteins in the lens [2, 3]. The only available treatment for cataract is eye surgery, which is costly and it is not risk-free. Developed countries like the United States spend billions of dollars per year in cataract surgery, while in developing countries cataract has become the major cause of visual disability [4].

Congenital cataracts are due to mutations in the genes that code for lens crystallin proteins [5], while sporadic cataract disease is caused by damage to these proteins throughout lifetime, including oxidation, deamidation, glycation, racemization and truncation [2, 6-9]. Covalent modifications of crystallins can lead to the formation of partially folded intermediates that are prone to non-amyloid aggregation [2, 3]. Crystallins are classified as:  $\alpha$ -crystallins, which are multimeric molecular chaperones belonging to the family of small heat shock proteins; the dimeric and oligomeric  $\beta$ -crystallins, and the monomeric  $\gamma$ -crystallins [3, 10, 11].  $\alpha$ -crystallins are able to recognize partially folded damaged  $\beta$ - and  $\gamma$ - crystallins, binding them to prevent their aggregation [2, 12]. The lens is formed of elongated fiber cells with high protein content, depleted of nuclei and organelles; this unique cell differentiation occurs in the embryonic stage [13]. Fully differentiated fiber cells have a very low metabolism, and are unable to synthesize new proteins, nor to degrade damaged lens proteins. Thus, in an aged lens,

when the chaperone  $\alpha$ -crystallins are depleted, further damage to lens crystallins cause development of cataract. Indeed, cataract incidence is strongly associated with aging.

Native  $\gamma$ -crystallins are highly soluble and stable, but *in vitro* chemical or thermal denaturation have shown to lead to the formation of partially folded intermediates that are prone to aggregation [2, 3]. The N-terminal domain has shown to be less stable, as compared to the C-terminal domain [14]. Studies of mutations associated to congenital cataract have also shed light into the mechanisms of the non-amyloid aggregation of  $\gamma$ -crystallins [15-19]. Overall, a domain swapping mechanism has been proposed, involving interactions between partially destabilized crystallins [2]. Interestingly, a recent structural study has identified the conservation of a native-like fold in non-amyloid aggregates of a cataract-associated mutation in human  $\gamma$ D-crystallin [20]. Thus, small perturbations in the protein fold and stability of  $\gamma$ -crystallins may be enough to cause non-amyloid aggregation, while a native-like fold is preserved.

A variety of studies have implicated metals as a potential etiological agent in cataract disease. Cataract is well documented among workers in metal-working industries [21]. The concentration of metal ions, such as copper and zinc, in cataractous lenses are increased significantly, as compared to normal lenses, suggesting a potential role of these essential metals in cataract disease [22-24]. Indeed, metal ion levels in the human lens change upon normal aging and can also be influenced by habits, such as smoking [24, 25]. Smoking is a major risk factor for cataract disease [26, 27], and it is well documented as a major source of metals, such as cadmium and lead [28]. Accumulation of copper, lead and cadmium has been identified in cataractous lenses from cigarette smokers [24, 25]. On the other hand, environmental exposure and elevated blood levels

of mercury have been associated to an increased risk for age-related cataract disease [29]. These observations suggest a potential role of heavy metal ions in cataract disease pathology. Environmental exposure to heavy metal ions - e.g. from airborne particles from glass manufacturing [30]- is indeed a public concern, as xenobiotic metals such as lead, cadmium and mercury can hijack the trafficking mechanisms in place for essential metal ions in the human body, accumulating in several tissues and causing a variety of toxic effects through oxidative mechanisms [31].

The interaction of metal ions with lens crystallin proteins has been relatively unexplored. Essential metal ions such as Cu(II) and Zn(II) are known to bind to the chaperone  $\alpha$ -crystallins [32-35], while they can also induce the non-amyloid aggregation of human  $\gamma$ D-crystallin (H $\gamma$ D), one of the more abundant  $\gamma$ -crystallins in the core of the lens [36]. In particular, the mechanism of copper-induced aggregation of H $\gamma$ D crystallin involves loss of protein stability and formation of partially folded intermediates that lead to high molecular weight light-scattering aggregates. Metal-induced aggregation of H $\gamma$ D crystallin involves site-specific interactions with the protein, revealing a novel bioinorganic facet of cataract disease. In this study, we expand these investigations to evaluate the impact of heavy metal ions in the stability and aggregation of  $\gamma$ -crystallins.

The monomeric  $\gamma$ -crystallins are structural lens proteins that contain four Greek key motifs organized into two domains [3]. The mammalian genome contains seven  $\gamma$ -crystallin genes; the  $\gamma$ -A-F-crystallin genes are most copiously expressed in early lens development, thus their products are mainly found in the lens core region, while  $\gamma$ S-crystallin is expressed solely in the cortical region of the lens [5]. The human  $\gamma$ D-,  $\gamma$ S- (H $\gamma$ S), and  $\gamma$ C- (H $\gamma$ C) crystallins are among the most abundant structural proteins in the

human lens, comprising 11%, 9% and 7%, respectively, of the total protein content in young human eye lenses [37]. In this study, we use these three  $\gamma$ -crystallin proteins as a case study to explore the effects of heavy metal ions, such as Pb(II), Hg(II), Cd(II), in protein stability and aggregation, events that could be associated with the mechanisms of toxicity of heavy metal ions and particularly with the potential role of these metals in the development of cataract disease.

## Materials and Methods

**Plasmids and site-directed mutagenesis.** Plasmids encoding **tagless** H $\gamma$ C, H $\gamma$ D, and H $\gamma$ S crystallins were used. For H $\gamma$ C and H $\gamma$ D crystallins, pET16b **plasmids lacking the His tag were used**, as previously described [38-41]. For H $\gamma$ S crystallin, the coding sequence was amplified from a pQE1-H $\gamma$ S plasmid [42], flanked by NcoI and XhoI restriction enzyme sites. The H $\gamma$ S insert was ligated into a pET15b NcoI/XhoI plasmid, using a Gibson Assembly kit (New England Biolabs), yielding a **tagless** H $\gamma$ S construct. For H $\alpha$ B-crystallin a pAED4 plasmid was used, as previously described [43].

Site-directed mutagenesis of  $\gamma$ -crystallins was performed using a Q5 site-directed mutagenesis kit from BioLabs. Table S1 lists the oligonucleotide primers used for each mutation. The DNA plasmids obtained after mutagenesis were sequenced with the T7 promoter primer and were found to contain the desired mutation but no other sequence changes.

**Recombinant human  $\gamma$ -crystallin expression and purification.** Recombinant H $\gamma$ C, H $\gamma$ D, and H $\gamma$ S crystallins were expressed in BL21-RIL E. Coli, and purified by ammonium sulfate precipitation followed by size exclusion chromatography (SEC), as previously described [36, 38-41]. Briefly, this involves growing cells at 37 °C in super broth to an optical density of  $\sim$ 5 at 600 nm. Protein expression was induced with 1 mM isopropyl  $\beta$ -D-1-thiogalactopyranoside (ITPG) at 18 °C overnight. Harvested cells from a 2 L culture growth were resuspended with 10 mM ammonium acetate buffer pH 7, 50 mM NaCl, to a total volume of 50 mL. Cells were lysed by incubation with lysozyme (1 mg/mL) and DNase (20 ng/mL) for 30 min, in the presence of EDTA-free Complete-mini



protease inhibitor cocktail (Roche), followed by 10-15 sonication cycles (30 s each) in ice. Lysate was centrifuged at 17,000 g for 45 min, and ammonium sulfate was slowly added to the supernatant to reach 30% (w/v), while stirring in ice. The proteins that precipitated at 30 % ammonium sulfate were discarded, and more ammonium sulfate was added to reach 50% (w/v) and cause  $\gamma$ -crystallin precipitation. The precipitate was resuspended in 10 mM ammonium acetate buffer pH 7, with 50 mM NaCl, spun down, and passed through a 0.2  $\mu$ m filter before loading into a SEC column (Hi-Prep Sephacryl S-100), using a fast protein liquid chromatography (FPLC) instrument (GE Life Sciences). Eluted  $\gamma$ -crystallin fractions were analyzed by SDS-PAGE to verify purity, pooled and stored at 4 °C. Protein concentration was determined by electronic absorption spectroscopy, using the extinction coefficient  $\epsilon = 41 \text{ cm}^{-1} \text{ mM}^{-1}$  for all  $\gamma$ -crystallins.

**Turbidity Assays.** Crystallin proteins (50  $\mu$ M) were incubated in 10 mM ammonium sulfate buffer pH 7.0 with 50 mM NaCl, in the absence or presence of metal ions, at 37 °C (unless otherwise stated), in a total volume of 200  $\mu$ L. **Metal ions were added to the buffer solutions and pre-equilibrated at 37°C before addition of the protein.** Samples were incubated and analyzed in a FluoStar Optima 96-well plate reader. Absorbance at 400 nm was monitored every 60 s, shaking 10 s before each measurement. CdCl<sub>2</sub>, Pb(NO<sub>3</sub>)<sub>2</sub> and HgCl<sub>2</sub> salts were used as source of Cd(II), Pb(II) and Hg(II) ions; however, it should be noted that no effect of the counter-ion was observed, as mercury or cadmium acetate and lead chloride salt yielded identical results. No turbidity was detected in the control experiments with protein in sample buffer, nor for sample buffer with 10 equiv of metal ions in the absence of protein. For each experiment, kinetic traces were baseline corrected

using the control trace of sample buffer only. Turbidity assays were run at least four times for each condition.

**Transmission Electron Microscopy.** Protein aggregates from the end point of turbidity assays were diluted by 2-fold with water, incubated onto glow-discharged carbon coated Cu-Formvar grids (Ted Pella) for 1 min, blotted with filter paper, stained with uranyl acetate (1.5 % w/v) for 30 s, and dried. Grids were imaged in a Jeol-1400 EX transmission electron microscope.

**CD Spectroscopy.**  $\gamma$ -crystallins were characterized by circular dichroism, in the absence and presence of Hg, Cd or Pb ions. Independent solutions of 2  $\mu$ M protein in 5 mM potassium phosphate buffer pH 7.0 with 5 mM NaCl with the indicated amount of metal ion were prepared. CD spectra were collected in a Jasco J-815 CD spectropolarimeter.

**UV-Visible Absorption Spectroscopy.** Room temperature absorption titrations were recorded using an Agilent 8453 diode array spectrometer at room temperature. A 1 cm path length quartz cell was used, and spectra were recorded between 200 and 400 nm sampling points. Independent solutions of 5  $\mu$ M protein in 5 mM potassium phosphate buffer pH 7.0 with 5 mM NaCl with the indicated amount of metal ion were prepared.

## Results and Discussion

### 1. Hg(II) ions specifically induce the aggregation of H $\gamma$ C and H $\gamma$ S crystallins, but not H $\gamma$ D crystallin.

The effect of adding 0 to 10 equiv of Pb(II), Cd(II) or Hg(II) ions to a 50  $\mu$ M solution of H $\gamma$ D, H $\gamma$ C or H $\gamma$ S crystallin was evaluated by turbidity assays (Figure S1). In these assays, an increase in turbidity reports the formation of large light-scattering protein aggregates. While Pb(II) and Cd(II) had very small effects in the aggregation of these proteins, Hg(II) ions specifically induced significant aggregation of H $\gamma$ C and H $\gamma$ S crystallins, but not H $\gamma$ D crystallin **at the protein concentration used** (Figures 1A-C). It should be noted that the effect of the Hg(II) ions is independent on the counter anion used (Figure S2). Although these  $\gamma$ -crystallins are homologous and have a double Greek key fold with high  $\beta$ -sheet content (Figure 1D), it is very interesting to note that H $\gamma$ D crystallin is not susceptible to Hg-induced aggregation, in spite of its homology with the other two  $\gamma$ -crystallins. The nature of the Hg-induced aggregates is non-amyloid, as probed by electron microscopy (Figures 1E-F). Turbidity assays reveal that the extent of Hg-induced aggregation of H $\gamma$ C and H $\gamma$ S crystallins highly depends on the metal:protein ratio, but with distinct features for each protein (Figure 2). For H $\gamma$ S crystallin, the extent of aggregation increases steadily with the number of equiv of Hg(II) added and saturates at 4 equiv (Figure 2B and blue trace in Figure 2H). This behavior indicates that there is a metal-dependent event that initiates mercury-induced aggregation of H $\gamma$ S crystallin, and it saturates at 4 equiv of metal ion. In contrast, Hg-induced aggregation of H $\gamma$ C crystallin reaches a maximum at 3 equiv of metal ion and then it significantly decreases at higher metal:protein ratios (Figure 2A and blue trace in Figure 1G), revealing that different

competing mechanisms may be at work, with opposing effects on the mercury-induced aggregation of H $\gamma$ C crystallin.

## **2. Hg(II) ions induce loss of thermal stability and secondary structure of H $\gamma$ C and H $\gamma$ S crystallins.**

Thermal denaturation experiments on H $\gamma$ C and H $\gamma$ S crystallins were performed to assess the impact of Hg(II) ions in the thermal stability of these proteins. This was assessed by circular dichroism (CD) spectroscopy, monitoring the intensity of the negative signal at 218 nm that is indicative of  $\beta$ -sheet secondary structure, as a function of the temperature of the protein sample. H $\gamma$ C and H $\gamma$ S crystallins are stable proteins that can be heated up to 70 °C with no apparent effect on their secondary structure. However, at higher temperatures the CD signal at 218 nm decreases significantly, indicating thermal denaturation. Figures 2C and 2D show thermal denaturation curves for H $\gamma$ C and H $\gamma$ S crystallin, respectively, expressing the fraction of the protein that has unfolded as a function of temperature. The midpoint of each curve corresponds to the temperature at which approximately half of the protein retains its native conformation ( $T_m$ ). For H $\gamma$ S crystallin, a  $T_m = 76.78 \pm 0.16$  °C can be determined (Figure 2D and Table S2), consistent with previous reports [44]. However, when the thermal denaturation experiment is performed in the presence of 1 to 10 equiv of Hg(II) ions, the value of the  $T_m$  significantly decreases (down to  $48.01 \pm 0.02$  °C for 10 equiv), while the shape of the curve is also affected (Figure 2D and Table S2). The impact of Hg(II) ions in the thermal stability of H $\gamma$ S crystallin is directly proportional to the metal:protein ratio, as shown in the red trace in Figure 2H, while it is inversely proportional to the extent of aggregation

observed at the end point of the turbidity assay at each metal concentration (blue trace in Figure 2H).

In contrast, thermal denaturation experiments of H $\gamma$ C crystallin in the presence of 1 to 10 equiv of Hg(II) ions display a distinct behavior (Figure 2C and Table S2). A  $T_m = 80.38 \pm 0.05$  °C can be determined for H $\gamma$ C crystallin in the absence of metal ions. However, while the first 3 equiv of Hg(II) induce a drastic loss of thermal stability ( $T_m$  decreases to  $43.31 \pm 0.05$  °C for 3 equiv), the addition of 4, 5 or 10 equiv of metal ion have a milder impact on the  $T_m$  value (Figure 2C and Table S2); in fact, the  $T_m$  at 10 equiv of Hg(II) recovers to  $59.05 \pm 0.02$  °C. The biphasic behavior of the thermal stability of H $\gamma$ C crystallin as a function of metal:protein ratio (red trace in Figure 2G) is inversely proportional to the biphasic behavior of the extent of aggregation observed at the end point of the turbidity assay at each metal concentration (blue trace in Figure 2G). In fact the two traces correlate well, indicating that at 3 equiv of Hg(II) ions there is a maximum of Hg-induced aggregation that is likely due to a minimum in thermal stability at such metal:protein ratio. This correlation reveals that very distinct Hg-protein interactions must be occurring at low (< 3 equiv of Hg) and high (> 3 equiv) metal:protein ratios, leading to the formation of different metal-protein complexes with competing effects on thermal stability and extent of Hg-induced aggregation of H $\gamma$ C crystallin.

CD spectroscopy was also used to evaluate the impact of Hg(II) ions in protein folding. Titrations of H $\gamma$ C and H $\gamma$ S crystallin with the metal ion were followed by CD at 20 °C, as shown in Figures 2E and 2F, respectively. For H $\gamma$ S crystallin, the addition of 1 to 4 equiv of Hg(II) ions causes a gradual and mild decrease on the intensity of the 218 nm negative CD signal, indicating loss of  $\beta$ -sheet secondary structure (Figure 2F). A trace of the

remaining folded fraction is plotted against the number of equiv of metal ion in Figure H, and it correlates well with the loss of thermal stability in the first 4 equiv of Hg(II). The loss of secondary structure also correlates well with an increase in the extent of Hg-induced aggregation of H $\gamma$ S crystallin, as in both cases the effects reach a plateau at 4 equiv of metal ion. Overall, these results indicate that the key Hg-protein interactions that lead to loss of protein folding, decreased thermal stability, and metal-induced aggregation of H $\gamma$ S crystallin must occur upon addition of the first 4 equiv of metal ion.

On the other hand, for H $\gamma$ C crystallin, while the addition of the first 3 equiv of Hg(II) causes a drastic decrease on the intensity of the 218 nm negative CD signal, indicating the loss of ~40% of the secondary structure, the addition of more equivalents have little further effect (Figure 2E and green trace in Figure 2G). It should be noted that the drastic loss of secondary structure caused by the first equivalents of Hg(II) ions correlate well with a loss of thermal stability and an increased Hg-induced aggregation of H $\gamma$ C crystallin, reaching a maximum at 3 equiv (Figure 2G). Thus, these results indicate that the metal-protein interactions that occur at low metal:protein ratios (< 3 equiv of Hg) must be associated to partial unfolding of the protein, loss of thermal stability and Hg-induced aggregation of H $\gamma$ C crystallin.

### **3. Differential effects of Hg(II) ions in the N- and C- terminal domains of H $\gamma$ C and H $\gamma$ S crystallins.**

In order to gain further insight into the mechanism of Hg-induced aggregation of H $\gamma$ C and H $\gamma$ S crystallins, the impact of this metal ion in the aggregation, folding and thermal stability of the separate domains of the proteins was evaluated (Figures 3&4). Constructs for the separate N- and C- terminal domains of each protein could be produced, yielding

stable proteins that do not aggregate, even after incubation at 37 °C (black traces in Figures 3A-B and 4A-B). However, turbidity assays show that both, the N-terminal and the C-terminal domains of both crystallins are susceptible to mercury-induced aggregation. The differential effects of Hg(II) ions on the domains are discussed below for each protein.

For HyC crystallin, the N- (Figure 3A) and C-terminal (Figure 3B) domains are both prone to Hg-induced aggregation, the extent of aggregation increases with the metal:protein ratio and saturates after 2 or 3 equiv of Hg(II) (blue traces in Figures 3G&H). Interestingly, none of the domains show the biphasic behavior displayed by the full protein (Figures 2A&G). Thermal denaturation experiments with the separate domains of HyC crystallin in the presence of 0 to 4 equiv of Hg(II) ions are shown in Figures 3C&D. A  $T_m = 73.02 \pm 1.44$  °C can be determined for the N-terminal domain, while the value for the C-term is  $T_m = 74.14 \pm 1.81$  °C. In both cases, the addition of Hg(II) ions cause a decrease in thermal stability (Figures 3C&D, Table S3); however, in contrast to that observed in the full protein, no biphasic behavior was observed (red traces in Figures 3G&H). These results clearly indicate that the metal-protein interactions that lead to the biphasic behavior in Hg-induced aggregation and loss of thermal stability require both domains to be present. Finally, the impact of Hg(II) ions in the protein folding of each domain was assessed by CD spectroscopy at 20 °C. For both, the N-term (Figure 3E) and the C-term (Figure 3F) domains, the addition of mercury causes a gradual and mild decrease on the intensity of the 218 nm negative CD signal, indicating loss of  $\beta$ -sheet secondary structure. However, the extent of Hg-induced protein unfolding is much larger in the N-terminal domain, for which only 50% of the protein remains

folded upon addition of > 4 equiv of Hg(II) ions; as compared to the C-term domain, where 70% of the protein remains folded even after the addition of 5 equiv of metal ion (green traces in Figures 3G and 3H).

Overall, these results indicate that the mechanism of Hg-induced aggregation of the separate domains of H $\gamma$ C crystallin involves loss of thermal stability and protein folding, although the impact on the folding is significantly larger for the N-terminal domain. However, most importantly, the interesting biphasic behavior observed for the Hg-induced aggregation of the full protein (Figure 2G) is abolished when the experiment is performed with the separate domains. Thus, the metal-protein interactions that occur at higher metal:protein ratios and lead to a decreased effect in aggregation must involve **interactions between both domains** of H $\gamma$ C crystallin.

On the other hand, the N- (Figure 4A) and C-terminal (Figure 4B) domains of H $\gamma$ S crystallin are also both prone to Hg-induced aggregation. While the extent of aggregation of the N-terminal domain increases gradually with the metal:protein ratio, the effect on the C-term domain saturates after 2 or 3 equiv of Hg(II) (blue traces in Figures 4G&H). Thermal denaturation experiments show that the addition of Hg(II) ions cause a drastic decrease in thermal stability for both domains (Figures 4C&D, Table S4). Although a lower  $T_m$  value ( $65.12 \pm 1.56$  °C) can be determined for the N-terminal domain, as compared to that of the C-terminal domain ( $T_m = 73.22 \pm 0.5$  °C), the addition of the first equiv of Hg(II) yields a drastic decrease in both domains, down to  $27.08 \pm 0.79$  and  $30.02 \pm 1.96$  °C, respectively. Finally, the addition of mercury also causes a gradual and mild decrease on the intensity of the 218 nm negative CD signal at 20 °C, indicating loss of  $\beta$ -sheet secondary structure for both, the N-term (Figure 4E) and the C-term (Figure 4F)



domains. Similarly to the case of H $\gamma$ C crystallin, the extent of Hg-induced protein unfolding is much larger in the N-terminal domain of H $\gamma$ S crystallin, for which only 50% of the protein remains folded upon addition of > 3 equiv of Hg(II) ions; as compared to the C-term domain, where 70% of the protein remains folded even after the addition of 5 equiv of metal ion (green traces in Figures 4G and 4H). Overall, **these** results indicate that the mechanism of Hg-induced aggregation of the separate domains of H $\gamma$ S crystallin involves loss of thermal stability and protein folding, although the impact on the folding is significantly larger for the N-terminal domain.

**4. Hg(II) ions induce formation of disulfide-bridged dimers involving the N-terminal domains.** SDS-PAGE analysis of the Hg-induced aggregates of H $\gamma$ C and H $\gamma$ S crystallins was performed; in both cases, the denatured aggregates led to a very intense band at ~20 kDa, which corresponds to the molecular weight of the monomeric proteins (Figures 5A and 5D, respectively). These results indicate that the metal-induced aggregates are composed of mostly monomeric units of  $\gamma$ -crystallin. However, a second band at ~37 kDa was also detected at higher Hg:protein ratios (red arrows in Figures 5A&D), which might correspond to a dimeric species. The intensity of the band at ~37 kDa is very faint for the H $\gamma$ C aggregates (Figure 5A), while it is significantly more intense for H $\gamma$ S crystallin and it appears at Hg:protein ratios higher than 3 equiv (Figure 5D). It is important to note that this band at ~37 kDa completely disappears when the SDS-PAGE analysis of the Hg-induced aggregates is performed in the presence of reducing agents, such as  $\beta$ -mercaptoethanol (data not shown), suggesting that these dimeric species may be disulfide bridged.

The Hg-induced aggregates of the separate domains of both proteins were also analyzed by SDS-PAGE (Figures 5 B, C, E&F). In all cases, a very intense band at ~10 kDa is observed, which corresponds to the molecular weight of the monomeric domains. However, a second species is also observed between 15 and 20 kDa, only in the Hg-induced aggregates of the N-terminal domains of H $\gamma$ C (Figure 5B) and H $\gamma$ S (Figure 5E) crystallins. These bands might correspond to disulfide-bridged dimeric species for each domain, since they are no longer observed when the SDS-PAGE analysis is performed in the presence of  $\beta$ -mercaptoethanol (data not shown). Similarly to the case of the full proteins, the presence of disulfide-bridged species is much more evident for the N-terminal domain of H $\gamma$ S at Hg:protein ratios higher than 2 equiv (Figure 5E), as compared to H $\gamma$ C (Figure 5B). It is important to note that SDS-PAGE analysis of aggregates formed with the C-terminal domains does not display any disulfide-bridged species (Figures 5C&F).

Overall these results suggest that the mechanism of Hg-induced aggregation of H $\gamma$ C and H $\gamma$ S crystallins may involve formation of disulfide-bridged dimeric species, where amino acid residues at the N-terminal domains of these proteins may be engaged.

**5. Putative Hg(II) binding sites and mechanisms of Hg-induced aggregation of H $\gamma$ C and H $\gamma$ S crystallins.** Hg(II) ions have a preference to coordinate soft ligands, such as Cys residues, usually in a bi-coordinate fashion. Indeed, preliminary electronic absorption data of titrations of H $\gamma$ C and H $\gamma$ S crystallins with Hg(II) ions display ligand to metal charge transfer (LMCT) bands at ~ 297 nm (~ 33,670 cm<sup>-1</sup>) and ~ 235 nm (~ 42,550 cm<sup>-1</sup>), which are indicative of Cys sulfur-based coordination to Hg ions (Figure S3) [45]. A more detailed spectroscopic characterization of the interactions of Hg(II) ions

with H $\gamma$ C and H $\gamma$ S crystallins would be needed to elucidate the coordination modes involved; however, it is clear that Cys sulfur-based ligands are involved in Hg(II) coordination.

$\gamma$ -crystallins contain several Cys residues (Scheme 1 and Figure 6). H $\gamma$ D crystallin contains a total of 6 Cys residues. Two of them, Cys 109 and 111, are located in the C-terminal domain, and are arranged in a way that they could accommodate a linear bi-coordinate geometry. Since this pair of Cys residues is absent in H $\gamma$ C and H $\gamma$ S crystallins, where only Cys109 is conserved, we speculate that the Cys109/Cys111 pair might be a binding site for Hg(II) ions in H $\gamma$ D crystallin that does not cause aggregation. In contrast, for H $\gamma$ C and H $\gamma$ S crystallins, their C-terminal domains have a second Cys residue that is solvent exposed (Cys153 and Cys130, respectively), which could engage in metal-bridging mechanisms. Indeed, our results indicate that the mechanism of Hg-induced aggregation of the C-terminal domains does not involve di-sulfide bridged species and it has a smaller contribution of partial unfolding events (as compared to the N-terminals); thus, it is likely that the dominant mechanism at the C-terminal domains involves the formation of metal-bridged species (Figure 7).

On the other hand, the N-terminal domains of  $\gamma$ -crystallins generally contain a higher number of Cys residues, as compared to their C-terminal domains; and these residues are present in a localized region of the protein (Figure 6). While the N-terminal domain of H $\gamma$ D crystallin only contains 4 Cys residues, and two of them are in an arrangement that could accommodate a bi-coordinate Hg(II); H $\gamma$ C and H $\gamma$ S crystallins have five Cys residues, and most of them are clustered in a solvent-exposed region of the N-terminal domain. In particular, it is interesting to note that Cys22 is conserved in H $\gamma$ C and H $\gamma$ S

crystallins, while that residue is a His22 in HyD crystallin, which is not susceptible to Hg-induced aggregation; thus, it is tempting to propose that having a Cys residue at position 22 may be key for the Hg-induced aggregation of HyC and HyS crystallins, and perhaps the formation of disulfide-bridged species at the N-terminal region. HyC and HyS crystallin aggregates only contain monomeric or disulfide-bridged dimers, while no evidence for covalently linked higher molecular weight species was observed. This observation, along with the fact that only the N-terminal domains of these proteins can yield disulfide-bridged species, strongly suggests that the disulfide bridge in the dimeric species must be formed between N-terminal Cys residues of two monomers, leading to a closed dimer (Figure 7). Further aggregation of these dimeric species likely involves metal bridging mechanisms using Cys residues from the C-terminal domains, as discussed above.

Our results indicate that Hg-induced unfolding plays an important role in metal-induced aggregation of  $\gamma$ -crystallins, and this phenomenon is more pronounced at the N-terminal domain, consistent with the fact that this domain is more susceptible to loss of protein folding, as compared to the C-terminal domain [14]. Several Cys residues engaged in  $\beta$ -sheet secondary structural elements could be identified in the structures of HyC and HyS crystallins. A unique arrangement for a Cys pair, Cys78 and Cys79, contained in a  $\beta$ -sheet structure is found in HyC crystallin, and it might be the structural motif responsible for the drastic Hg-induced unfolding observed in this protein upon addition of the first 3 equiv of metal ion. Interestingly, these two Cys residues were found to form a disulfide bond in a lens proteomic study [46]. Cys 41 and Cys129 constitute another unique Cys pair in HyC crystallin (Figure 6), which is located at the interface between the N- and C-

terminal domains. It is likely that the Cys41/Cys129 pair is responsible for the unique biphasic behavior observed in Hg-induced aggregation of H $\gamma$ C crystallin, as this protein is the only  $\gamma$ -crystallin with such a unique pair. Bi-coordinate Hg(II) coordination at this site might strengthen the inter-domain interaction, leading to the stabilizing effects observed for H $\gamma$ C crystallin at metal:protein ratios higher than 3 equivalents (Figure 7). This proposal is consistent with the observation that the biphasic behavior was abolished when using the separate domains.

## Conclusions

In this study we have evaluated the effect of heavy metal ions in the protein stability and aggregation of three of the more abundant  $\gamma$ -crystallin proteins in the human lens: H $\gamma$ D, H $\gamma$ C and H $\gamma$ S crystallins. Our study reveals that Hg(II) ions specifically induce the non-amyloid aggregation of H $\gamma$ C and H $\gamma$ S crystallins, while H $\gamma$ D crystallin is not sensitive to this metal ion. Mercury-induced aggregation of H $\gamma$ C and H $\gamma$ S crystallins occurs through diverse mechanisms including: metal-induced loss of stability and partial unfolding of the proteins, formation of disulfide-bridged dimeric species, and potentially through metal-bridging pathways (Figure 7). The interaction of Hg(II) with these  $\gamma$ -crystallins likely involves Cys residues, especially at the Cys-rich N-terminal domains of H $\gamma$ C and H $\gamma$ S, where the metal ion causes partial unfolding of the protein. Further spectroscopic and site-directed mutagenesis studies must shed light into the nature of these mercury-crystallin interactions and their role in the mechanism of metal-induced protein aggregation. While Hg ions are not normally present in a healthy human lens, environmental exposure to this metal is a concern; and since crystallins in the core of the

lens are not replaced, a one-time exposure would be enough to damage lens proteins. Thus, this study points to a potential role of this xenobiotic metal ion in the development of cataract, underscoring the bioinorganic facet of this disease.

### **Acknowledgements**

This research has been supported by the National Council for Science and Technology in Mexico (CONACYT grant # 221134 to L.Q. and fellowships to J.A.D.C.), MIT-Seed Funds, NIH EY015834 grant to J.A.K., and Fulbright-García Robles fellowship and Cátedra Marcos Moshinsky to L.Q. Authors would like to thank the technical assistance of Cammeron Haase-Pettingell (at MIT) and Lourdes Rojas at the Unit of Microscopy (Cinvestav).

### **References**

- 1 WHO. (2015) Visual impairment and blindness. 2015. [Http://www.Who.Int/mediacentre/factsheets/fs282/en/](http://www.Who.Int/mediacentre/factsheets/fs282/en/). Cited January 18, 2017
- 2 K. L. Moreau and J. A. King (2012) Trends in Mol Med 18:273-282
- 3 E. Serebryany and J. A. King (2014) Prog Biophys Mol Biol 115:32-41
- 4 Deloitte Access Economics (2014) The economic cost and burden of eye diseases and preventable blindness in Mexico. <https://www2.deloitte.com/content/dam/Deloitte/au/Documents/Economics/deloitte-au-economics-cost-eye-diseases-280314.pdf>.
- 5 J. Graw (2009) Exp Eye Res 88:173-189
- 6 P. G. Hains and R. J. W. Truscott (2010) Invest Ophthalmol Vis Sci 51:3107-3114
- 7 K. Lampi, P. A. Wilmarth, M. R. Murray and L. L. David (2014) Prog Biophys Mol Biol 115:21-31
- 8 T. Takata, J. T. Oxford, B. Demeler and K. Lampi (2008) Protein Sci 17:1565-1575
- 9 T. Takata, K. Murakami, A. Toyama and N. Fujii (2018) Biochim Biophys Acta 1866:767-774
- 10 M. P. Haslbeck, J.; Buchner, J.; Weinkauff, S. (2016) Biochim Biophys Acta 1860:149-166
- 11 V. K. Vendra, I.; Chandani, S.; Muniyandi A.; Balasubramanian, D. (2016) Biochim Biophys Acta 1860:333-343
- 12 L. Acosta-Sampson and J. King (2010) J Mol Biol 401:134-152

- 13 M. A. Wride (2011) *Philos Trans R Soc B-Biol Sci* 366:1219-1233
- 14 M. S. Kosinski-Collins and J. King (2003) *Protein Sci* 12:480-490
- 15 E. Serebryany and J. A. King (2015) *J Biol Chem* 290:11491-11503
- 16 E. Serebryany, J. C. Woodard, B. V. Adkar, M. Shabab, J. A. King and E. I. Shakhnovich (2016) *J Biol Chem* 291:19172-19183
- 17 E. Serebryany, T. Takata, E. Erickson, N. Schafheimer, Y. Wang and J. A. King (2016) *Protein Sci* 25:1115-1128
- 18 D. Khago, E. K. Wong, C. N. Kingsley, J. A. Freites, D. J. Tobias and R. W. Martin (2016) *Biochim Biophys Acta* 1860:325-332
- 19 K. W. Roskamp, D. M. Montelongo, C. D. Anorma, D. N. Bandak, J. A. Chua, K. T. Malecha and R. W. Martin (2017) *Invest Ophthalmol Vis Sci* 58:2397-2405
- 20 J. C. Boatz, M. J. Whitley, M. Li, A. M. Gronenborn and P. C. A. van der Wel (2017) *Nature Comm* 8:15137
- 21 H. Donald (1962) *The diseases of occupations*. Little, Brown and Co.,
- 22 J. Dawczynski, M. Blum, K. Winnefeld and J. Strobel (2002) *Biol Trace Elem Res* 90:15-23
- 23 V. K. Srivastava, N. Varshney and D. C. Pandey (1992) *Acta Ophthalmol* 70:839-841
- 24 O. Cekic (1998) *British J Ophthalmol* 82:186-188
- 25 A. Langford-Smith, V. Tilakaratna, P. R. Lythgoe, S. J. Clark, P. N. Bishop and A. J. Day (2016) *PLoS One* 11:e0147576
- 26 J. R. Chang, E. Koo, E. Agron, J. Hallak, T. Clemons, D. Azar, R. D. Sperduto, F. L. Ferris and E. Y. Chew (2011) *Ophthalmology* 118:2113-2119
- 27 J. Ye, J. He, C. Wang, H. Wu, X. Shi, H. Zhang, J. Xie and S. Y. Lee (2012) *Invest Ophthalmol Vis Sci* 53:3885-3895
- 28 A. Saffari, N. Daher, A. Ruprecht, C. De Marco, P. Pozzi, R. Boffi, S. H. Hamad, M. M. Shafer, J. J. Schauer, D. Westerdahl and C. Sioutas (2014) *Environ Sci: Processes Impacts* 16:2259-2267
- 29 M. Lemire, M. Fillion, B. Frenette, A. Mayer, A. Philibert, C. J. Sousa Passos, J. R. Davee Guimaraes, F. Barbosa Jr. and D. Mergler (2010) *Environ Health Perspect* 118:1584-1589
- 30 <https://www.documentcloud.org/documents/2771769-Memo-From-Janet-McCabe-on-Art-Glass-Manf.html#document/p2/a284265>.
- 31 C. Garza-Lombo, Y. Posadas, L. Quintanar, M. E. Gonsebatt and R. Franco (2018) *Antioxid Redox Signal* 28:1669-1703
- 32 M. F. Ahmad, D. Singh, A. Taiyab, T. Ramakrishna, B. Raman and C. M. Rao (2008) *J Mol Biol* 382:812-824
- 33 A. Biswas and K. P. Das (2008) *Biochemistry* 47:804-816
- 34 A. Laganowsky, J. L. P. Benesch, M. Landau, L. Ding, M. R. Sawaya, D. Cascio, Q. Huang, C. V. Robinson, J. Horwitz and D. Eisenberg (2010) *Protein Sci* 19:1031-1043
- 35 A. Mainz, B. Bardiaux, F. Kuppler, G. Multhaup, I. C. Felli, R. Pierattelli and B. Reif (2012) *J Biol Chem* 287:1128-1138
- 36 L. Quintanar, J. A. Dominguez-Calva, E. Serebryany, L. Rivillas-Acevedo, C. Haase-Pettingell, C. Amero and J. A. King (2016) *ACS Chem Biol* 11:263-272

- 37 N. E. Robinson, K. J. Lampi, J. P. Speir, G. Kruppa, M. Easterling and A. B. Robinson (2006) *Mol Vision* 12:704-711
- 38 Y. P. Wang, S.; Trojanowski, T.; Knee, K.; Goulet, D.; Mukerji, I.; and King, J. (2010) *Invest Ophthalmol Vis Sci* 51:672-678
- 39 A. P. Pande, J.; Asherie, N.; Lomakin A.; Ogun, O.; ‡, King J.; Benedek G. B. (2001) *PNAS* 98:6116-6120
- 40 A. Pande, Pande, j.; Asherie, N.; Lomakin, A.; Ogun†, o.; King J. A.; Lubsen N. H.; Walton, D.; Benedek G. B. (2000) *PNAS* 97:1993-1998
- 41 L. Fu and J. J. N. Liang (2002) *FEBS letters* 513:213-216
- 42 I. A. Mills, S. L. Flaugh, M. S. Kosinski-Collins and J. A. King (2007) *Protein Sci* 16:2427-2444
- 43 T. X. Sun, B. K. Das and J. J. Liang (1997) *J Biol Chem* 272:6220-6225
- 44 Z. Ma, G. Piszczek, P. T. Wingfield, Y. V. Sergeev and J. F. Hejtmancik (2009) *Biochemistry* 48:7334-7341
- 45 M. Luczkowski, M. Stachura, V. Schirf, B. Demeler, L. Hemmingsen and V. L. Pecoraro (2008) *Inorg Chem* 47:10875-10888
- 46 S. R. Hanson, D. L. Smith and J. B. Smith (1998) *Exp Eye Res* 67:301-312

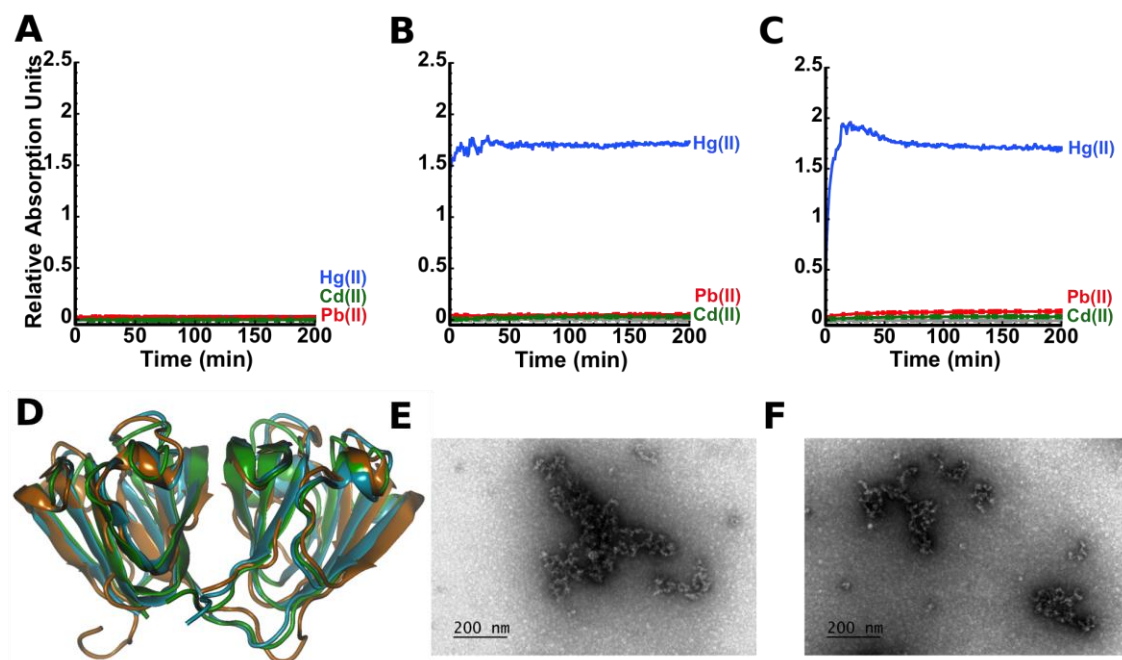


**Figure 1.** Turbidity assays of H $\gamma$ D (A), H $\gamma$ C (B), H $\gamma$ S (C) crystallins (50  $\mu$ M) in the absence (gray trace) or presence of 6 equiv of Pb(II) (red trace), Cd(II) (green trace) or Hg(II) (blue trace). All assays were performed at 37  $^{\circ}$ C, and turbidity at 400 nm was followed after the addition of metal ion. A structure alignment of H $\gamma$ D (light blue), H $\gamma$ C (green) and H $\gamma$ S (orange) crystallins is shown in (D). Electron microscopy images for Hg-induced aggregates of H $\gamma$ C (E) and H $\gamma$ S (F) crystallins, at the end point of the turbidity assays with 4 equiv of Hg(II).





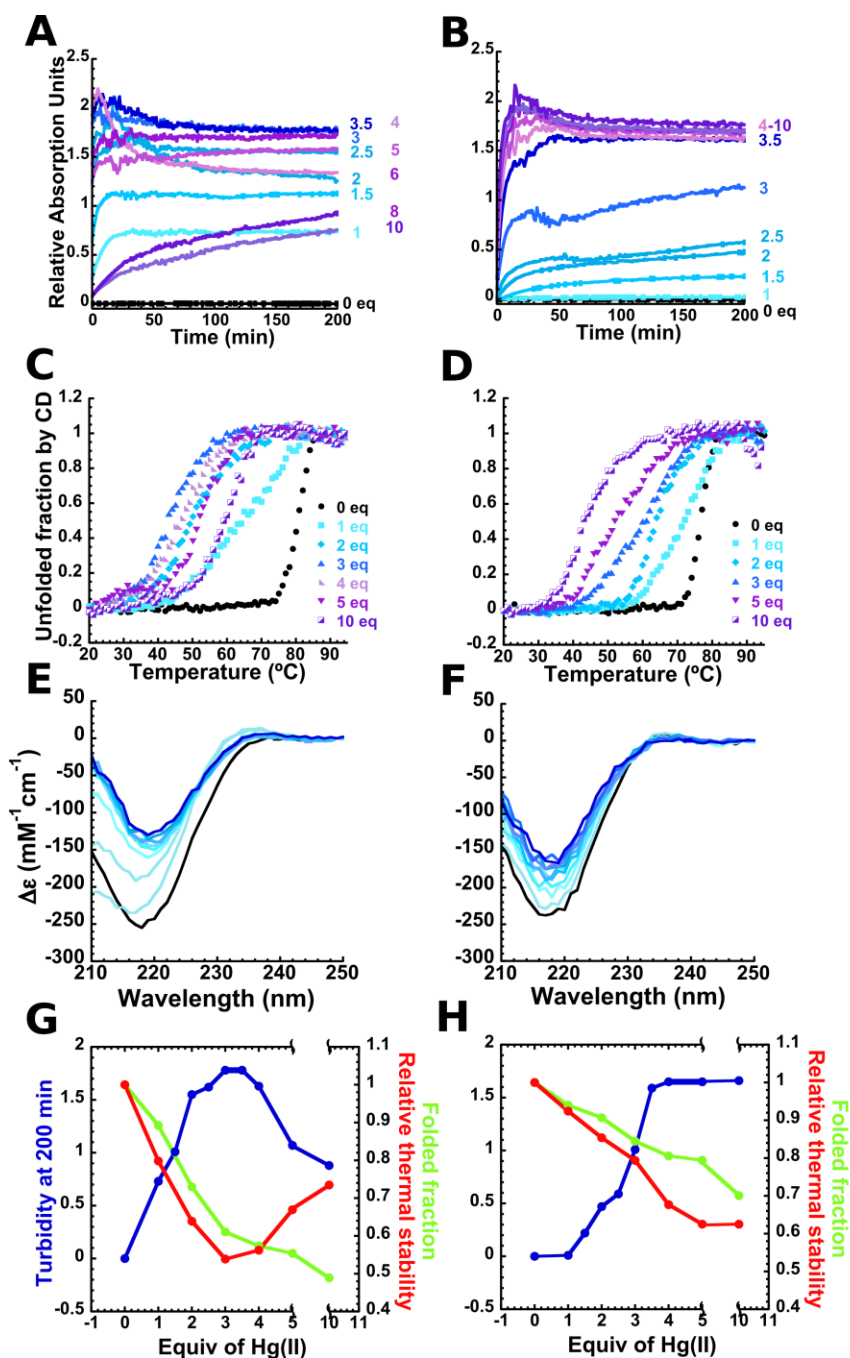


**Figure 2.** Turbidity assays of H $\gamma$ C (A) and H $\gamma$ S (B) crystallins (50  $\mu\text{M}$ ) in the absence (dark trace) or presence of 1, 1.5, 2, 2.5, 3, 3.5 (light to dark blue), 4, 5, 6, 8 and 10 equiv of Hg(II) (light to dark purple traces). All assays were performed at 37 °C, and turbidity at 400 nm was followed after the addition of Hg(II). Thermal denaturation of H $\gamma$ C (C) and H $\gamma$ S (D) crystallins (2  $\mu\text{M}$ ) was followed by CD in the presence of 0, 1, 2, 3, 4, or 5 equiv of Hg(II). The fraction of unfolded protein is plotted as a function of temperature, and the associated  $T_m$  values are listed in Table S2. Titrations of H $\gamma$ C (E) and H $\gamma$ S (F) crystallins (2  $\mu\text{M}$ ) with 0 (black spectra), 1, 2, 3, 4, 5, 6, 7, 8, 9 and 10 equiv of Hg(II) (light to dark traces), as followed by CD at 20 °C. Traces for turbidity, fraction of folded protein, and relative thermal stability, as a function of the number of equivalents of Hg(II) ions for H $\gamma$ C (G) and H $\gamma$ S (H) crystallins are also plotted.

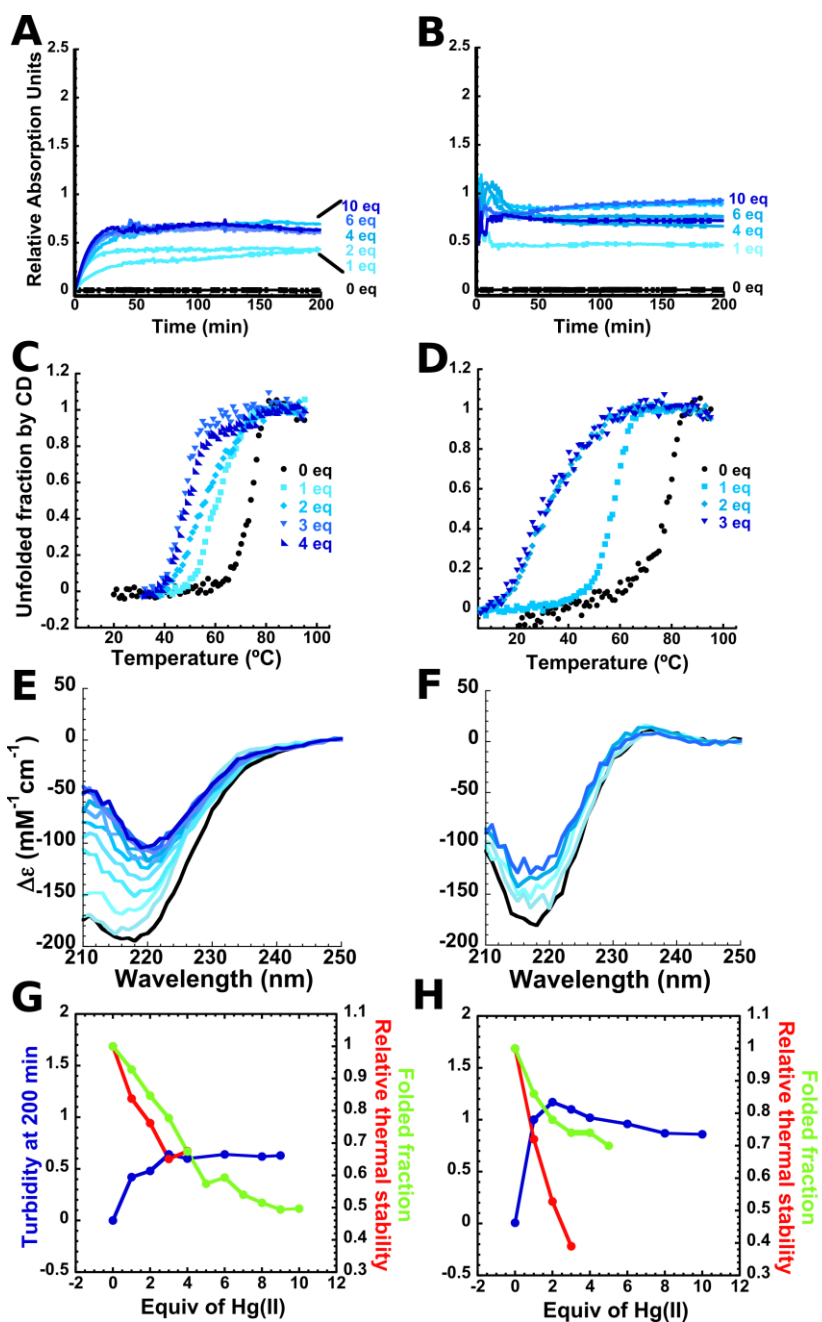


**Figure 3.** Turbidity assays of the N- (A) and C- terminal (B) domains of H $\gamma$ C crystallin (50  $\mu$ M) in the absence (black) or presence 1, 2, 4, 6, 8 and 10 equiv of Hg(II) (light to dark blue traces). All assays were performed at 37  $^{\circ}$ C, and turbidity at 400 nm was followed after the addition of Hg(II). Thermal denaturation of the N- (C) and C- terminal (D) domains of H $\gamma$ C crystallin (2  $\mu$ M) was followed by CD in the presence of 0, 1, 2, 3, 4, or 5 equiv of Hg(II). The fraction of unfolded protein is plotted as a function of temperature, and the associated  $T_m$  values are listed in Table S3.

Titration of the N- (E) and C- terminal (F) domains of H $\gamma$ C crystallin (2  $\mu$ M) with 0 (black), 1, 2, 3, 4, 5, 6, 7, 8, 9 and 10 equiv of Hg(II) (light to dark blue traces), as followed by CD at 20  $^{\circ}$ C. Traces for turbidity, fraction of folded protein, and relative thermal stability, as a function of the number of equivalents of Hg(II) ions for the N- (G) and C-terminal (H) domains of H $\gamma$ C crystallin are also plotted.

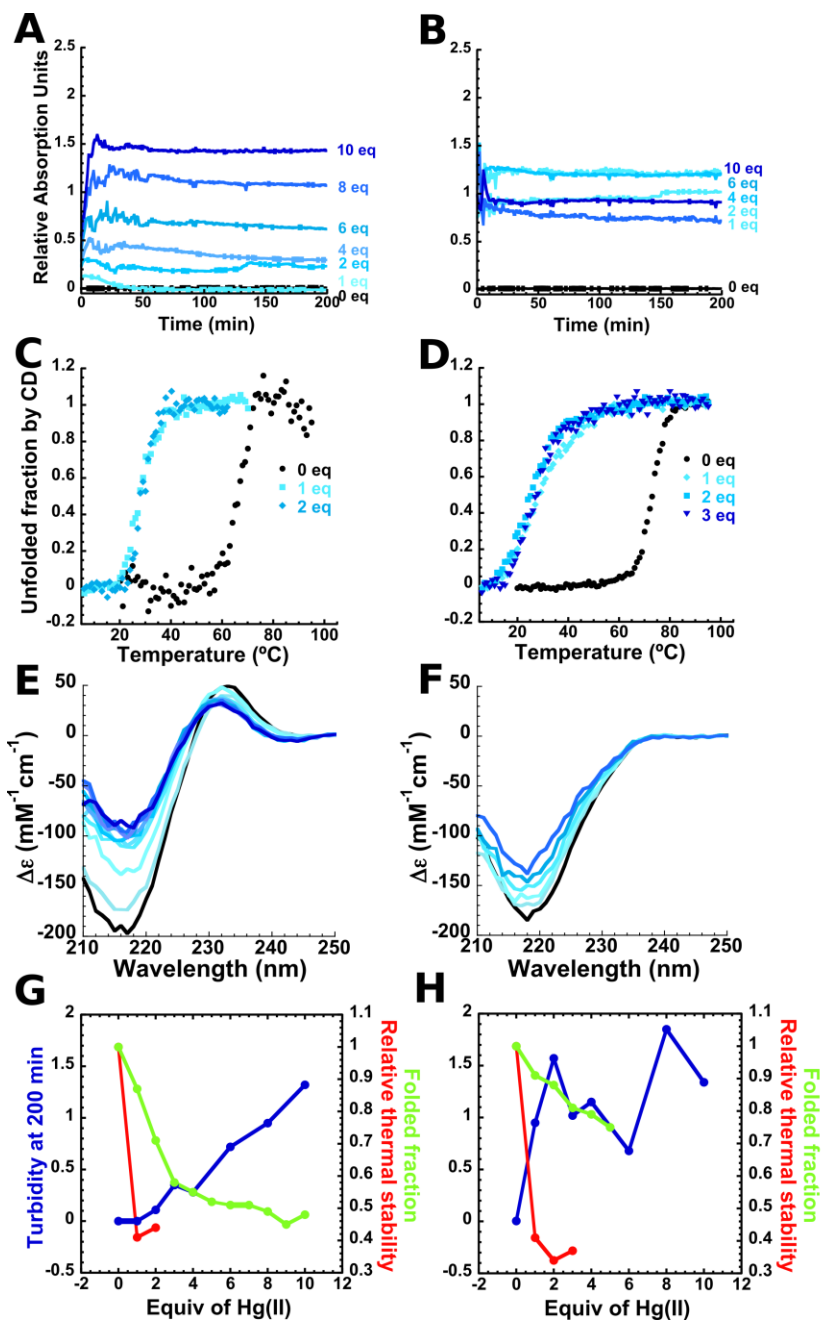


**Figure 4.** Turbidity assays of the N- (A) and C- terminal (B) domains of H $\gamma$ S crystallin (50  $\mu$ M) in the absence (black) or presence 1, 2, 4, 6, 8 and 10 equiv of Hg(II) (light to dark blue traces). All assays were performed at 37  $^{\circ}$ C, and turbidity at 400 nm was followed after the addition of Hg(II). Thermal denaturation of the N- (C) and C- terminal (D) domains of H $\gamma$ S crystallin (2  $\mu$ M)

was followed by CD in the presence of 0, 1, 2, 3, 4, or 5 equiv of Hg(II). The fraction of unfolded protein is plotted as a function of temperature, and the associated  $T_m$  values are listed in Table S4. Titrations of the N- (E) and C- terminal (F) domains of H $\gamma$ S crystallin (2  $\mu$ M) with 0 (black), 1, 2, 3, 4, 5, 6, 7, 8, 9 and 10 equiv of Hg(II) (light to dark blue traces), as followed by CD at 20 °C. Traces for turbidity, fraction of folded protein, and relative thermal stability, as a function of the number of equivalents of Hg(II) ions for the N- (G) and C-terminal (H) domains of H $\gamma$ S crystallin are also plotted.

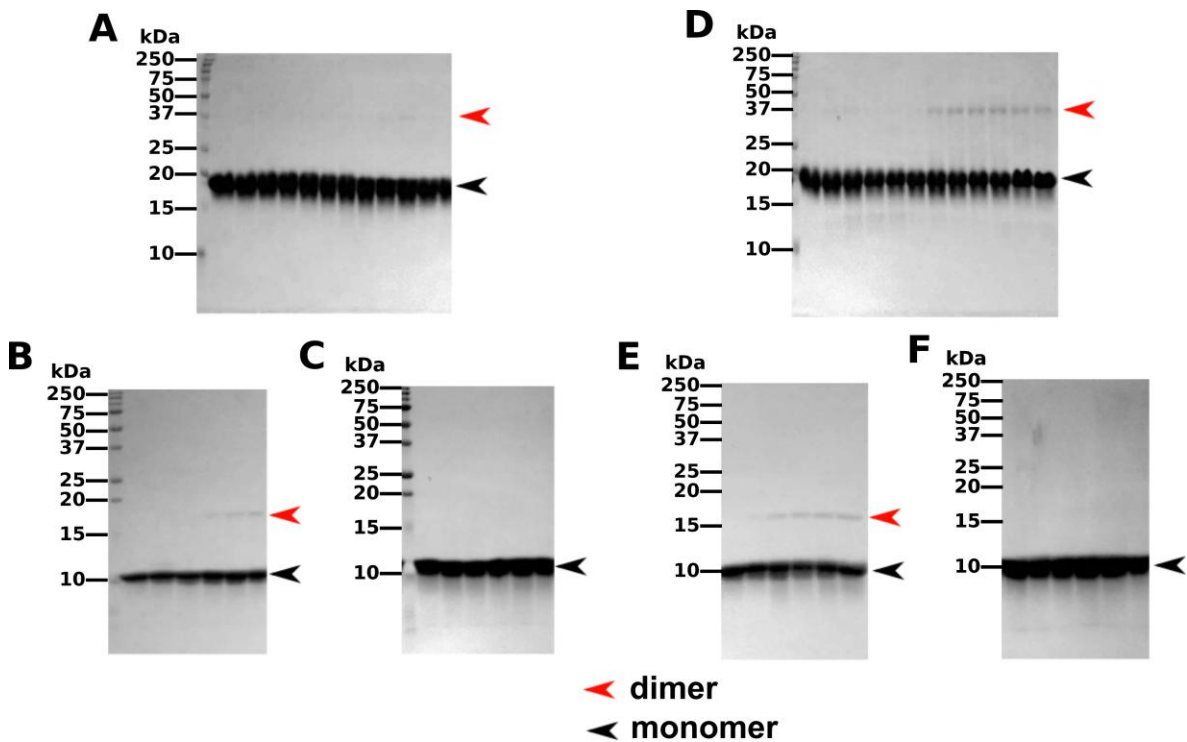


**Figure 5.** SDS-PAGE analysis of the metal-induced aggregates of wt (A), N- (B), and C- (C) terminal domains of H $\gamma$ C crystallin, and wt (D), N- (E), C- terminal (F) domains of H $\gamma$ S crystallin. Aggregates of wt H $\gamma$ C and H $\gamma$ S crystallins were obtained at the end of turbidity assays with increasing amounts of Hg(II) (0,1, 1.5, 2, 2.5, 3, 3.5, 4, 6, 8, and 10 equiv). Aggregates of N- (B and E) and C-terminal (C and F) domains of H $\gamma$ C and H $\gamma$ S crystallin were obtained at the end of turbidity assays with 2, 4, 6, 8, and 10 equiv of Hg(II). All aggregates were analyzed by SDS-PAGE after denaturation by boiling samples in SDS solutions without  $\beta$ -mercaptoethanol.

```

HyD Homo sapiens 1-173 1 -----GKITLYEDRGFQGRHYECSSDHPNLQPYLSRCNSARVDSGCWMLYEQPNYSGLQY 55
HyC Homo sapiens 1-173 1 -----GKITFYEDRAFQGRSYETTTDCPNLQPYFSRCNSIRVESGCWMLYERPNYQGGQY 55
HyS Homo sapiens 1-178 1 GSKTGTKITFYEDKNFQGRRYDCDCCADFHTYLSRCNSIKVEGGTWAVYERPNFAGYMY 60

HyD Homo sapiens 1-173 56 FLRRGDYADHQQWMGLSDSVRSCR--LIPHSGSHRIRLYEREDYRGQMIEFTEDCSCLQD 113
HyC Homo sapiens 1-173 56 LLRRGEYPDYQQWMGLSDSIRSCC--LIPQTVSHRLRLYEREDHKGLMMESEDCPSIQD 113
HyS Homo sapiens 1-178 61 ILPQGEYPEYQRWMGLNDRLSSCRAVHLPSSGGQYKIQIFEKGDFSGQMYETEDCPSIME 120

HyD Homo sapiens 1-173 114 RFRFNEIHSLNVLEGSWVLYELSNYRGRQYLLMPGDYRRYQDWGATNARVGSLRRVIDFS 173
HyC Homo sapiens 1-173 114 RFHLSEIRSLHVLEGCVVLYELPNYRGRQYLLRPQEYRRCQDWGAMDAKAGSLRRVVDLY 173
HyS Homo sapiens 1-178 121 QFHMREIHSCKVLEGVWIFYELPNYRGRQYLLDKKEYRKPIDWGAASPAVQSFRRIVE-- 178

```

**Scheme 1.** Sequence alignment of HyD (PDB: 1HK0), HyC (PDB: 2NBR) and HyS (PDB: 2M3T) crystallin proteins. All cysteine residues are highlighted with red color.

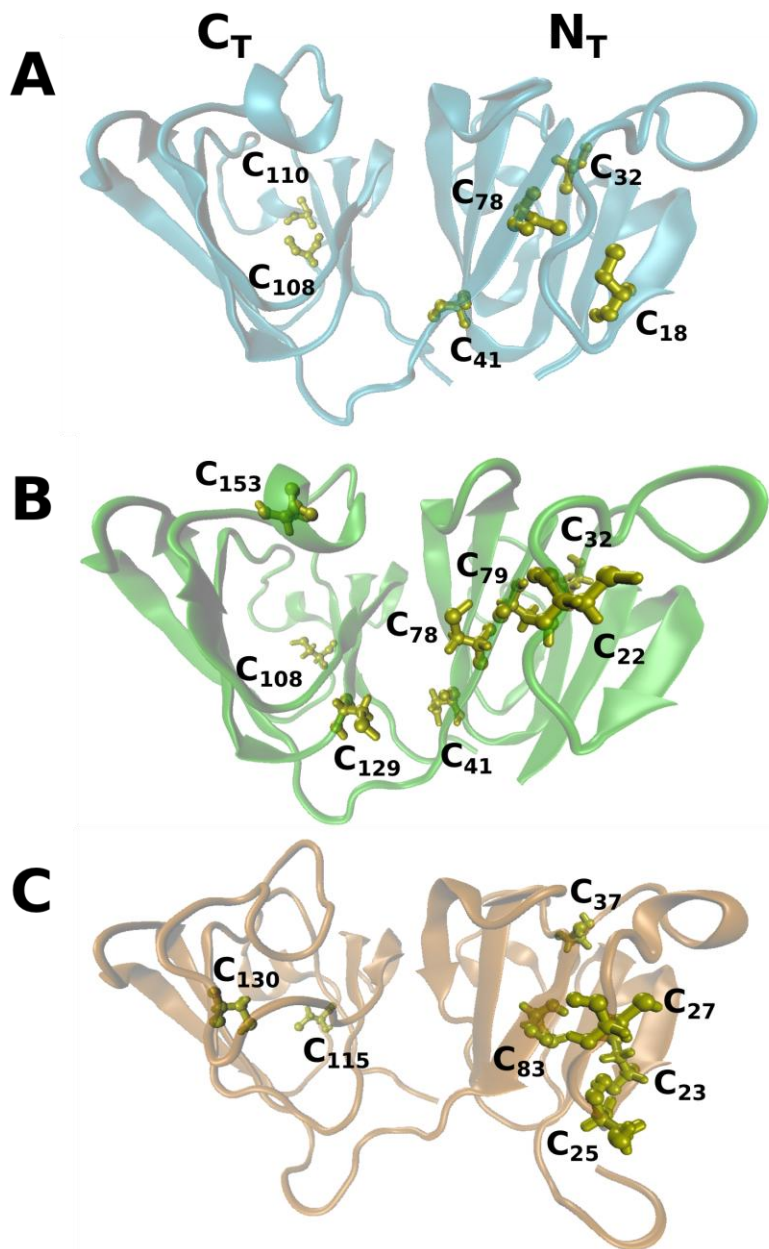


**Figure 6.** Structures of H $\gamma$ D (A), H $\gamma$ C (B) and H $\gamma$ S (C) crystallins, showing the positions of all cysteine residues in each protein.

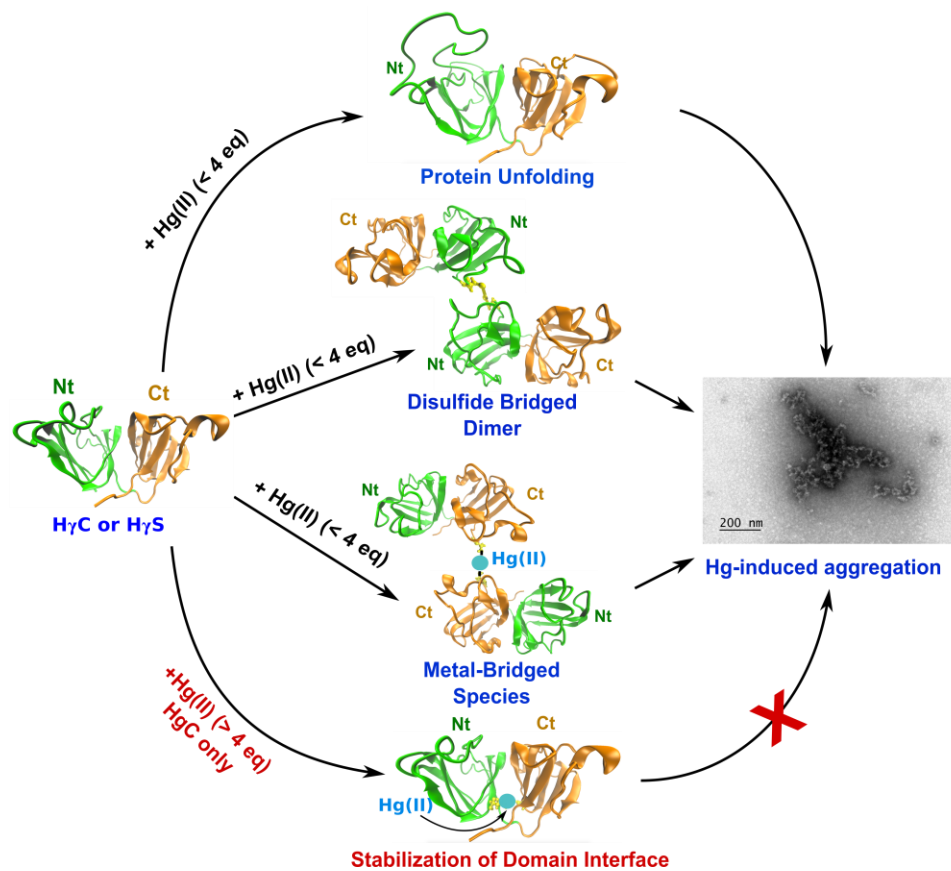
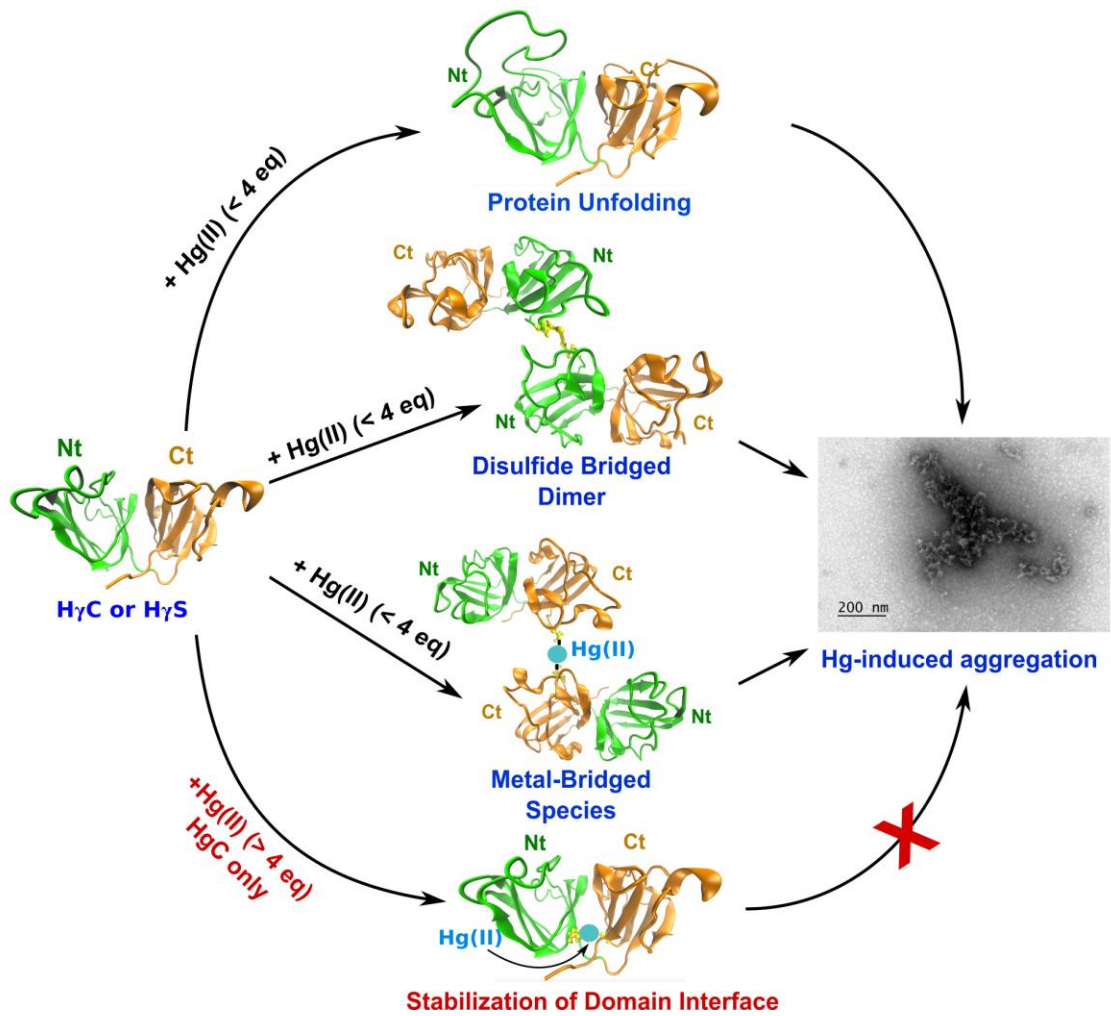


**Figure 7.** Proposed mechanisms for Hg(II)-induced aggregation of H $\gamma$ C and H $\gamma$ S crystallins. At low (< 4) equiv of metal ion, in both cases three mechanisms have been identified: i) loss of protein folding, predominantly at the N-terminal domain; ii) formation of disulfide-bridged dimers involving Cys residues from the N-terminal domain; and iii) formation of metal-bridged species, likely involving Cys residues from the C-terminal domain. For H $\gamma$ C crystallin, at high (>4 equiv) metal:protein ratios, interaction of Hg(II) with Cys residues in the domain interface stabilizes the protein and reduces metal-induced aggregation.





## Mercury-induced aggregation of human lens $\gamma$ -crystallins reveals a potential role in cataract disease

J. A. Domínguez-Calva,<sup>1</sup> M.L. Pérez-Vázquez,<sup>1</sup> E. Serebryany,<sup>2</sup> J. A. King,<sup>2</sup> L. Quintanar,<sup>1,\*</sup>

<sup>1</sup>Departamento de Química, Centro de Investigación y de Estudios Avanzados (Cinvestav), Mexico City, México

<sup>2</sup>Department of Biology, Massachusetts Institute of Technology, Cambridge, MA, USA

[lilianaq@cinvestav.mx](mailto:lilianaq@cinvestav.mx)

Keywords: lens crystallins, human gamma crystallin, mercury, heavy metal ions, cataracts disease

Table S1. Primers used for site-directed mutagenesis.

Mutation	Forward Primer	Reverse Primer
N-terminal domain of H $\gamma$ C crystallin	5'-TCTCATCCCCTAAACAGTCTCCC-3'	5'- CAACAGGAGCGGATGGAG -3'
C-terminal domain of H $\gamma$ C crystallin	5'- AGGCTGCGGCTGTACGAG -3	5'- CATGGTATATCTCCTTCTTAAAGTTAAACA AAATTATTC -3
N-terminal domain of H $\gamma$ S crystallin	5'- CAGAGCTGTTTAACTGCCTAGTGGAGG -3'	5'- CAGGAGCTGAGGCGGTCG -3'
C-terminal domain of H $\gamma$ S crystallin	5'-TATAAGATTCAGATCTTTGAGAAAG- 3'	5'- CATGGTATATCTCCTTCTTAAAG-3'

Table S2. Tm values for H $\gamma$ C and H $\gamma$ S crystallins in the presence of Hg(II) ions

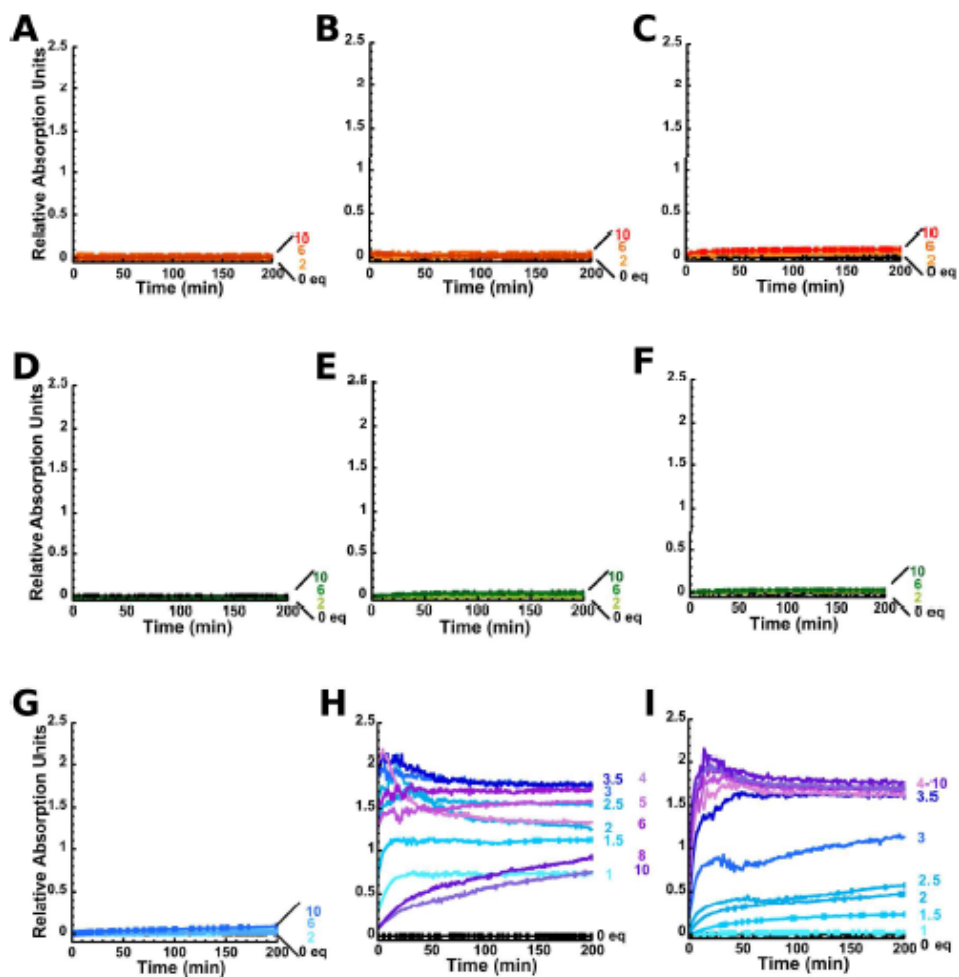
<b>Equiv of Hg(II)</b>	<b>Tm (°C) for H<math>\gamma</math>C</b>	<b>Tm (°C) for H<math>\gamma</math>S</b>
0	80.38 ± 0.05	76.78 ± 0.16
1	64.17 ± 0.10	70.97 ± 0.46
2	51.34 ± 1.50	65.57 ± 2.5
3	43.31 ± 0.05	60.94 ± 1.62
4	45.21 ± 1.50	48.83
5	53.81 ± 0.10	51.97 ± 1.26
10	59.05 ± 0.02	48.01 ± 0.02

Table S3. Tm values for N- and C-terminal domain of H $\gamma$ C crystallin in the presence of Hg(II) ions

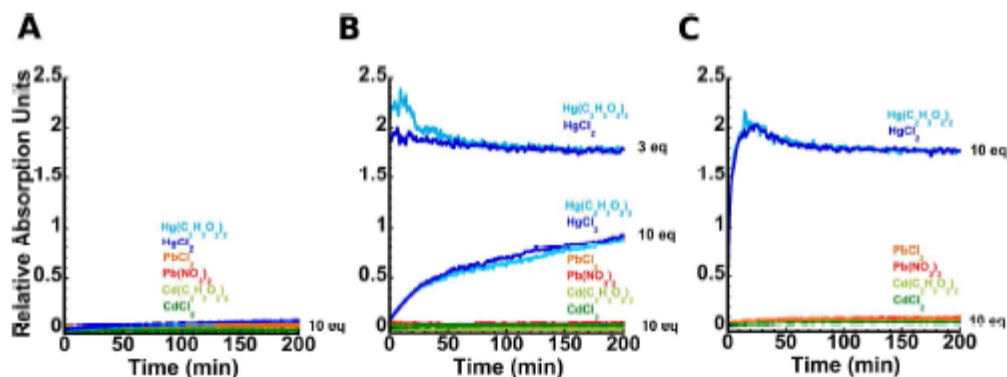
<b>Equiv of Hg(II)</b>	<b>Tm (°C) for N terminal</b>	<b>Tm (°C) for C terminal</b>
0	73.02 ± 1.44	74.14 ± 1.81
1	61.22 ± 0.47	53.56 ± 1.40
2	55.66 ± 0.91	39.12 ± 0.97
3	47.55 ± 0.83	29.27 ± 1.40
4	49.30 ± 0.05	-----

Table S4. Tm values for N- and C-terminal domain of H $\gamma$ S crystallin in the presence of Hg(II) ions

<b>Equiv of Hg(II)</b>	<b>Tm (°C) for N terminal</b>	<b>Tm (°C) for C terminal</b>
0	65.12 ± 1.56	73.22 ± 0.5
1	27.08 ± 0.79	30.02 ± 1.96
2	29.03 ± 1.50	25.5 ± 1.5
3	-----	27.33 ± 0.06



**Figure S1.** Turbidity assays of HyD (A, D, G), HyC (B, E, H), HyS (C, F, I) crystallins (50  $\mu$ M) in the absence (black) or presence of increasing number (1 to 10) of equivalents of Pb(II) (A, B, C), Cd(II) (D, E, F) or Hg(II) (G, H, I). All assays were performed at 37  $^{\circ}$ C, and turbidity at 400 nm was followed after the addition of metal ion.



**Figure S2.** Turbidity assays of HyD (A), HyC (B), HyS (C) crystallins (50  $\mu$ M) in the absence (black) or presence of different salts of Pb(II) (orange and red traces), Cd(II) (Green traces) or Hg(II) (blue traces). All assays were performed at 37  $^{\circ}$ C, and turbidity at 400 nm was followed after the addition of metal ion.

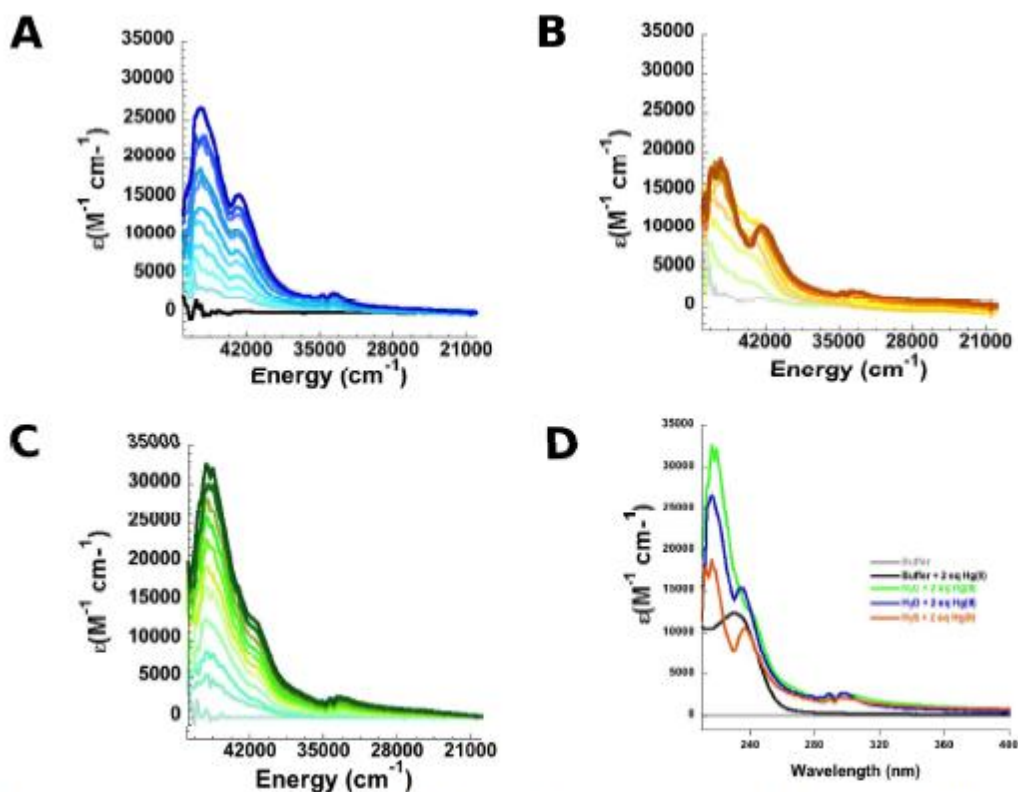


**Figure S3.** Titrations of HyD (A), HyS (B) and HyC (C) from 0.2 to 2.0 equiv of Hg(II), as followed by UV-vis absorption spectroscopy. Comparison of absorption spectra of buffer without (gray) or with 2 equiv of Hg(II) (black), and HyD (blue), HyC (green) or HyS (red) with 2 equiv of metal ion.